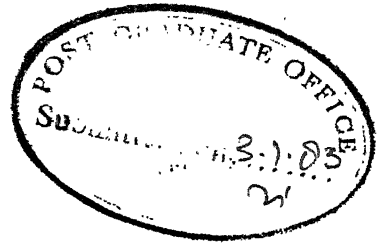


# **HIGH VELOCITY IMPACT PROPERTIES OF UNIDIRECTIONAL GFRP**

A Thesis Submitted  
In Partial Fulfilment of the Requirements  
for the Degree of  
**MASTER OF TECHNOLOGY**

**By**  
**R. K. NAKRANI**


to the  
**DEPARTMENT OF MECHANICAL ENGINEERING**  
**INDIAN INSTITUTE OF TECHNOLOGY, KANPUR**  
JANUARY, 1983




ii

### CERTIFICATE

This is to certify that this thesis entitled,  
"HIGH VELOCITY IMPACT PROPERTIES OF UNIDIRECTIONAL GFRP"  
submitted in partial fulfilment of the requirements for  
the Degree of Master of Technology by Mr. R.K. Nakrani,  
is a record of work carried out under our supervision and  
has not been submitted elsewhere for a degree.

  
Prashant Kumar  
Assistant Professor  
Deptt. of Mech. Engg.  
I.I.T. Kanpur

  
B.D. Agarwal  
Professor  
Deptt. of Mech. Engg.  
I.I.T. Kanpur

**25 MAY 1984**

**CENTRAL LIBRARY**  
*111, Kanpur.*

**Acc. No. A.....82427...**

To  
620.118  
111111

## ACKNOWLEDGEMENT

I express my deep sense of gratitude and appreciation to Dr. Prashant Kumar and Dr. B.D. Agarwal for their invaluable guidance and constant encouragement throughout the present work.

Credit is due to Mr. L.J. Rao, B.S. Patro, D.K. Sarkar and Y.V.V.S. Murthy for their active participation during the present work and for lending their hand when and where asked for.

I wish to express my sincere thanks to Mr. J.P. Parikh, V. Satish, J.R. Umaretiya and D.R. Parekh for their constructive suggestions and help whenever required.

I highly appreciate Mr. S.L. Srivastava, S.N. Yadav, R.S. Shukla, Shivaji Sarkar, O.P. Sachan and U.S. Tewari for their timely help during fabrication of experimental set-up and filament winding machine.

Thanks to Mr. B.K. Jain for his sincere efforts in preparing the illustrations.

Ramnik

## CONTENTS

ABSTRACT	v
LIST OF FIGURES	vi
CHAPTER 1 : INTRODUCTION	1
CHAPTER 2 : EXPERIMENTAL DETAILS	6
2.1 MATERIAL FABRICATION	6
2.2 TESTING SYSTEM	13
CHAPTER 3 : RESULTS AND DISCUSSIONS	23
CHAPTER 4 : SUMMARY AND CONCLUSIONS	42
REFERENCES	44

## ABSTRACT

An investigation of impact properties at high velocity on unidirectional glass/epoxy composite specimens were carried out. A filament winding machine was designed and fabricated to mould the unidirectional glass/epoxy composite. ( $V_F = 43.3\%$ ) of four different thicknesses. To study the response of the composite at high impact velocity (25.7 m/sec) a instrumented impact testing machine (Charpy type) was designed and fabricated. The effects of composite material are demonstrated. The testing machine gives a measure of matrix cracking in the form of the first kink in load history at about  $2/3$  of maximum load. Initiation energy, propagation energy, total impact energy and ductility index are affected by change in thickness. Failure mode changes with span-to-thickness ratio. Shear failure is observed in lower span-to-thickness ratio. The shear failure causes to split the specimen and can be treated as two specimens one over the other. For comparing the Charpy impact data span-to-thickness ratio is an important parameter.

## LIST OF FIGURES

Figure		Page
2.1	Schematic Diagram of Filament Winding Machine	7
2.2	Overall View of Filament Winding Machine	8
2.3	Microstructure of Unidirectional Glass/Epoxy Composite.	12
2.4	Schematic Diagram of Tup-Impact Experimental Set-up.	14
2.5	Close View of Tup-Impact Experimental Set-up	15
2.6	Overall View of Tup-Impact Experimental Set-up	16
2.7	Diagram of the Bridge Circuit with Passive Filter	19
3.1	Oscilloscope Records of Load History of Unidirectional Glass/Epoxy Composite for Different Thicknesses, h (a) 3.3 mm (b) 4.8 mm (c.) 6.4 mm. (d) 8.7 mm	24
3.2	Typical Load History During Tup Impact Test	25
3.3	Impact Load vs Thickness	27
3.4	Stress at Peak Load vs Thickness	28
3.5	Time vs Thickness	29
3.6	Effect on Energy Absorbed by GFRP	31
3.7	Influence of Thickness on Energy per Unit Thickness	33
3.8	Variation of Ductility Index with Thickness	34

Figure	Page
3.9 Photographs of the Two Sides of 3.3 mm Thick Unidirectional Impact Specimens. (a) Compression side (b) Tension side	36
3.10 Photograph of the Compression Side of 4.8 mm Thick Unidirectional Impact Specimens	37
3.11 Side View of 6.4 mm Thick Unidirectional Impact Specimens	39
3.12 Side View of 8.7 mm Thick Unidirectional Impact Specimens	40
3.13 Corrected Maximum Flexural Stress vs Thickness	41



## CHAPTER 1

### INTRODUCTION

The material having two or more distinct constituents or phases and having properties noticeably different from properties of its constituents is considered as a "Composite Material". A composite with fibre as one of its constituents is called fibre-reinforced composite and is one of the oldest and most widely used. In fibre-reinforced composite the strength, stiffness and other properties in different directions can be easily tailored to our needs by changing constituent materials, fibre orientation and other manufacturing variables. The potential for use of such composites for light weight structural engineering construction is well recognized.

The structural design using the fibre-reinforced plastics, FRP, requires the characterization of their behaviour under static and dynamic loading conditions because it is expected that the behaviour of the composites is different under the two loading conditions. In practice, we encounter dynamic loading conditions like a bird hitting an aircraft wing or a jet engine turbine blade. There are other such instances in truck cab, missile weapon system, motor car, railway car, highway guard rail. In view of this there is a need for fibre-reinforced composites to be tested for their impact strength.

The well known Charpy and Izod impact tests are widely used to evaluate impact properties to determine fracture toughness by measuring the fracture energy required. Chanis et al [1] , Novak and DeCrescento [2], Prewo [3], Agarwal and Narang [4] have studied the composite material using the conventional impact testing device. Transverse impact strength is found to be correlated with interlaminar shear strength [1] but in GFRP, resin matrix is an insignificant factor in energy absorption [2] and high impact level can be achieved with low matrix strength [3]. However, the impact energy of boron/aluminium composite material is dissipated mainly by plastic deformation of aluminium matrix [3] as it is ductile in nature. It is also observed that the impact energy reduces with the increasing angle between fibres and loading axis in glass/epoxy [4] . The impact energy can be correlated with the area under the fibre stress-strain curve [2].

The conventional impact tests are very useful for a comparative study of different materials. In advanced composite material the fracture phenomenon is more complex and hence the conventional tests are not sufficient for providing data of basic significance. This is because the particular mode of fracture determines various energy absorbing mechanisms operative during material failure under impact load. For better understanding, Charpy and Izod impact tests

are frequently instrumented to record the load history during the impact [5 - 9]. Toland [5] observed that the energy absorbed by carbon/epoxy and boron/epoxy composites is influenced by interfacial strength and also concluded that hybridization improves the impact resistance. He emphasised the difference between energy absorbed elastically and energy dissipated during failure. This is also supported by Beaumont et al [6] and a new parameter, the "Ductility Index", is proposed along with maximum stresses and total energy as a useful measure for comparing the impact performance of composite materials. They investigated unidirectional glass/epoxy, Kevlar-49/epoxy and graphite/epoxy. They observed that hybrid material (graphite-Kevlar/epoxy) has significantly higher ductility index and maximum stress than all-graphite fibre composite. Beaumont and Server [7] have investigated carbon/epoxy composite and observed that the fracture toughness depends upon the elastic characterization of the fibres. They also observed that crack propagation energy is controlled by the properties of interface. Adams and Miller [8] have compared the calculated elastic strain energy at maximum impact load with measured fracture initiation energy using graphite/epoxy composites. Pike and Novak [9] have shown importance of span-to-depth ratio in the interpretation of load and observed the influence of specimen thickness in terms of time to reach the maximum load level using the pendulum impact test (Charpy).

In the instrumented conventional tests, however, such test variables as impact velocity and available energy are held constant. This has resulted in the development of other types of impact testing systems such as drop-weight impact tests [10, 11]. Broutman and Rotem [10] have shown that the impact energy of unidirectional and cross-ply glass fibre laminates are strain rate sensitive in test range and orientation of the lamination is important. Mallick and Broutman [11] have investigated the effect of fibre orientation angle on the impact properties of glass/epoxy composites. They observed that the impact energy absorbed by cross-ply laminate is consistently higher than that for the unidirectional laminate except at  $0^\circ$  orientation. In other work [12], they have investigated impact behaviour of glass, Thronel-300 and Kevlar in an epoxy matrix and observed the increase in impact energy and ductility index in hybrid system and also observed dependence of the impact properties on type of fibre and interlaminar shear strength. Yeung and Broutman [13] have supported that the interlaminar shear strength plays an important role in transverse impact behaviour.

Aleszka [14] has investigated the dynamic response and corresponding damage resulting from localized impact loading on composite panels. Labor [15] observed that marginally visible impact damage reduces the static strength of composite panels.

The behaviour of a laminate is governed by individual unidirectional lamina. GFRP composites are increasingly being used for many engineering applications. It seems that reported impact properties, using conventional impact test and normal drop-weight impact test, are at low impact velocity. Hence present study is intended to study high velocity impact properties of unidirectional GFRP composite. For this purpose a projectile type instrumented impact testing machine is designed and fabricated. In this testing machine impact velocity can be varied over a wide range. The tup (projectile) represents a mass striking a composite structure and is instrumented to have load history during entire impact duration. The present study shows the successful use of the testing machine for testing composite material at high impact velocity. The impact strength of unidirectional GFRP composite has been investigated by performing the impact test at high impact velocity on unnotched specimens with impact load applied perpendicular to the plane of composite plate. The thickness parameter is considered and its effects on the impact behaviour and failure mechanism are studied.

## CHAPTER 2

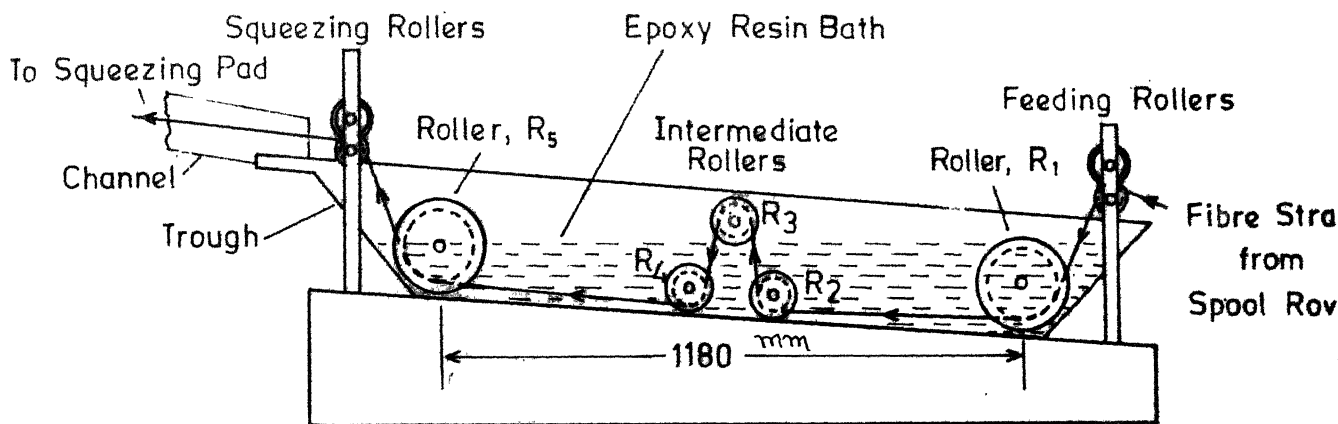
### EXPERIMENTAL DETAILS

#### 2.1 MATERIAL FABRICATION

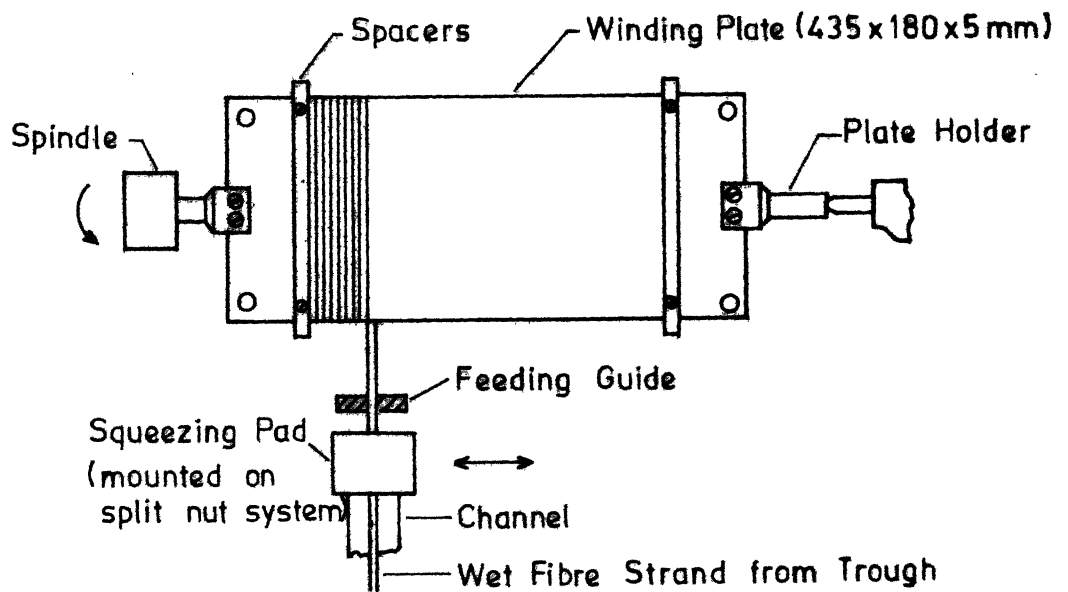
The present studies were carried out using epoxy resin as the matrix material and continuous glass fibre as the reinforcement. Epoxy resin (CY 230) and aliphatic amines as its curing agent (HY 951), manufactured and marketed by Ciba-Geigy of India Ltd, under the trade names 'Araldite' and 'Hardner' respectively, were used. Continuous E-glass fibres, a product of Fibreglass Pilkington Ltd. of India, were used as the reinforcement in the epoxy matrix.

A filament winding machine was designed and fabricated to mould unidirectional GFRP plates to get higher fibre volume fraction and to maintain good quality control. The schematic diagram and overall view of the filament winding machine is shown in Figs. 2.1 and 2.2. Fibres coming from spool roving were made to pass through the groove of a pair of feeding rollers. The depth and width of the groove in the female part of the feeding rollers was such that the fibre strand coming from a roving are seated comfortably in the groove. The feeding rollers were designed such that the clearance between two mating parts was 1 mm.

This fibre strand then passes through another set of rollers,  $R_1$  and  $R_5$ , which maintain the fibre strand dipping inside the epoxy resin bath (epoxy resin and 8%



(a)



(b)

Fig. 2.1. Schematic Diagram of Filament Winding Machine.

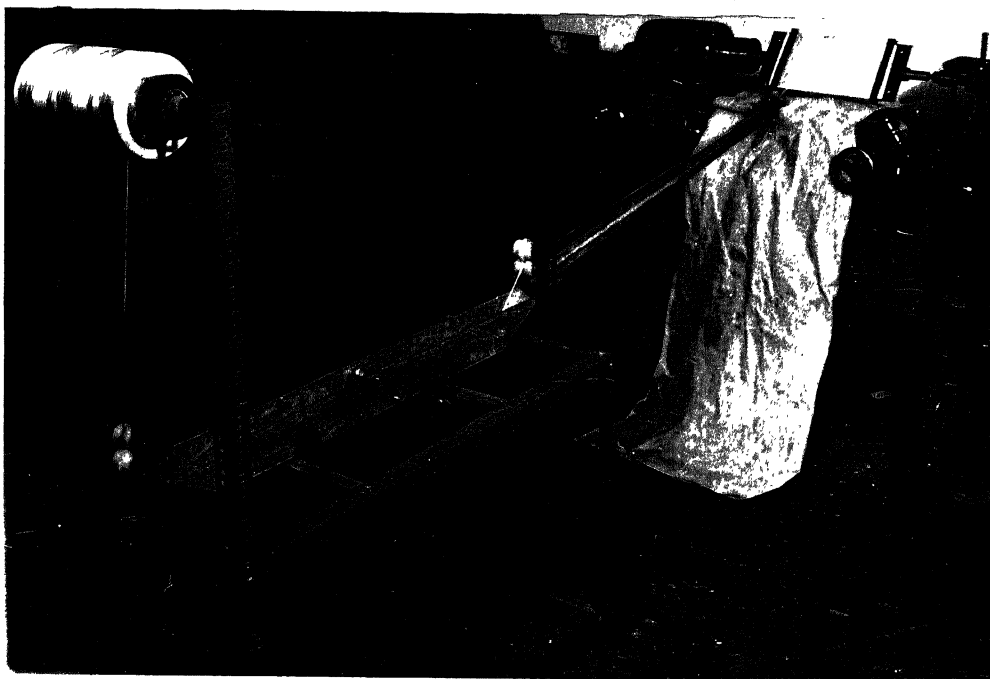


Fig. 2.2: Overall View of Filament Winding Machine



curing agent) in a trough. The intermediate rollers  $R_2$ ,  $R_3$  and  $R_4$ , kept between the rollers  $R_1$  and  $R_5$  to cause the epoxy resin to penetrate deep into the fibre strand. All five rollers have sufficient groove width to convert the fibre strand into a wide strip so as to increase its contact area with epoxy resin. The trough was slightly inclined rising towards the winding side, so that epoxy resin would not accumulate towards the winding side due to fibre strand and roller velocity. Thus, it improves the impregnation of fibre strand. The trough and the roller system is shown in Fig. 2.1 (a).

The fibre strand coming from epoxy resin bath passes through a pair of squeezing rollers which squeeze the fibre strand and remove some amount of excess epoxy resin. Then, the fibre strand was made to pass through a squeezing pad. The pressure of the squeezing pad on the fibre strand can be varied so that required amount of epoxy resin adheres to the fibre strand. The squeezing pad squeezes the fibre strand and removes the excess epoxy resin which is drained back to the trough through a channel. The squeezing pad and the channel are attached over a specially designed split-nut system fixed to the lead screw. Then, the fibre strand passes through a feeding guide (6.35 mm in width) is also attached over the split-nut system.

The fibre strand coming through feeding guide is fixed on a winding plate which is a smooth electroplated

M.S. one. The winding plate, with help of two plate holders was mounted on a mandrel. Mylar sheet and the spacers on either side of the winding plate are fixed. The mylar sheets are used to produce excellent surface finish. The squeezing pad, feeding guide and the winding plate is shown in Fig.

2.1 (b). The winding plate is rotated on a lathe machine and a traverse speed of split-nut system was kept at such level so that each fibre strand strip just touches the previous one. In the present case the plate revolved at 38 RPM and the traverse speed, kept at 4.022 m/sec (6.35 mm/rev. using 4 TPI), which exactly matches with the width of the feeding guide. The fibre strand traversed from one set of spacers to another give one layer and thereafter traversing direction is changed to have second layer. Rolling was done on both the sides of the winding plate for every two layers so that excess epoxy resin and air bubbles, if any, can be removed. The rolling can be done after any number of layers as and when required. Before the previous amount of epoxy resin gets emptied, freshly prepared epoxy resin was poured in the trough from time to time during the winding process. Likewise, one can wind number of layers as per requirement. In the present study, casting of plates with 10, 15, 20 and 28 layers of fibre strand was done to get 3.3, 4.8, 6.4 and 8.7 mm thick unidirectional GFRP plates for testing purpose. In fact, the filament winding machine is capable of producing

21 mm thick unidirectional GFRP plates with different fibre volume fraction.

After the winding was completed, two mylar sheets were kept on either side of the winding plate and was pressed in between two 25 mm thick MS casting plates. The spacers fixed on the winding plate control the thickness of the unidirectional GFRP plate. Curing was done at room temperature for 48 hours. After the curing was complete, GFRP plates were removed from winding plate by cutting out the material on both edges on diamond wheel-cutting machine. Casting at a time gives two identical unidirectional GFRP plates. Fibre volume fraction of these GFRP plates was approximately 43.3% as indicated by the burn-test. Variation in the thickness of a GFRP plate was found to be negligible. Figure 2.3 shows microstructure of the unidirectional GFRP plate fabricated using the filament winding machine.

Using above fabrication technique plates of size 250 mm x 150 mm were obtained. The specimens were cut from the plates on a diamond wheel-cutting machine. The length of the specimen is kept 120 mm in the direction of fibre and width of specimen is kept 10 mm in perpendicular direction.

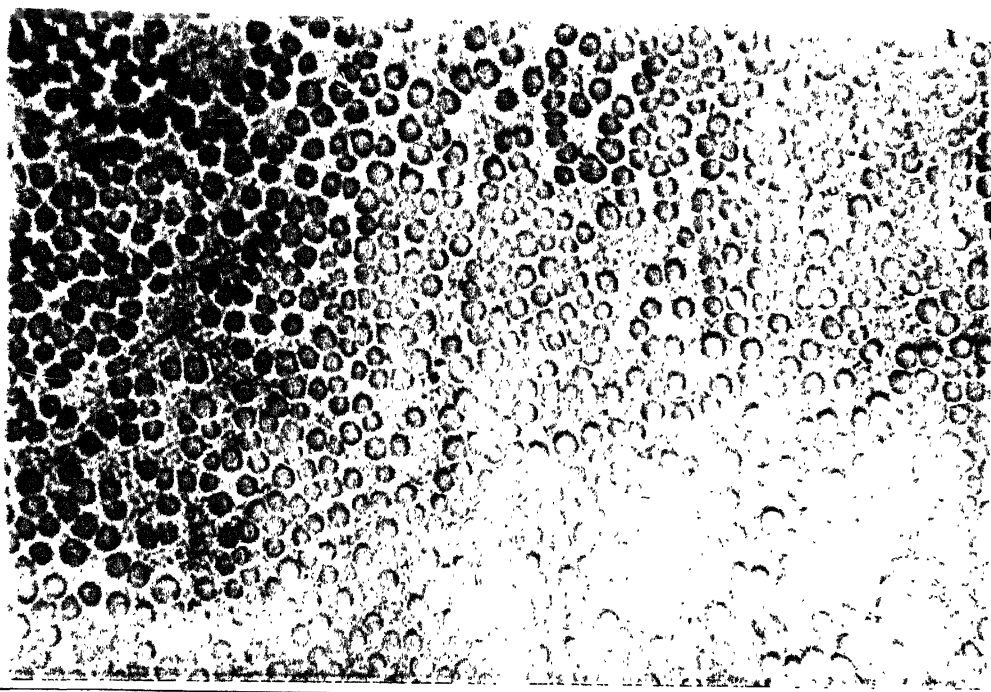


Fig. 2.3: Microstructure of Unidirectional Glass/Epoxy Composite

## 2.2 TESTING SYSTEM

In many applications, FRP are frequently subjected to impact loading. The inhomogeneity and the anisotropy in composite materials invite a wider set of failure mode. This may cause change in response to impact loading. Hence, it requires to know the ability of the material to withstand impact loading and the response to such loading. The impact strength of a material is defined as the energy required for fracture for unit cross-section during high speed loading. For this purpose a instrumented tup impact testing apparatus (Charpy type) is designed and developed to perform high velocity impact tests. The apparatus consists of air-gun, striker, tup, tup-guide, anvils and instrumentation part. The schematic diagram and the photographs of the experimental set-up are shown in Figs. 2.4 - 2.6 respectively.

A specimen is loaded dynamically in flexural mode by a tup which is hit by a striker (19.7 mm diameter and 198 mm long) which is made of EN-24 steel (IS: 40Ni 2Cr 1Mo 28). The striker is accelerated by an air-gun using high pressure nitrogen gas. The centre portion of the front face of the striker is made spherical so that it contacts tup at a point close to the centre. The tup is 135 mm long and has a square cross-section of 11 mm x 11 mm. The mass of the tup is 122.8 gms. The front of the tup is tapered to form a wedge of  $45^{\circ}$  angle with 3 mm tip radius to load the

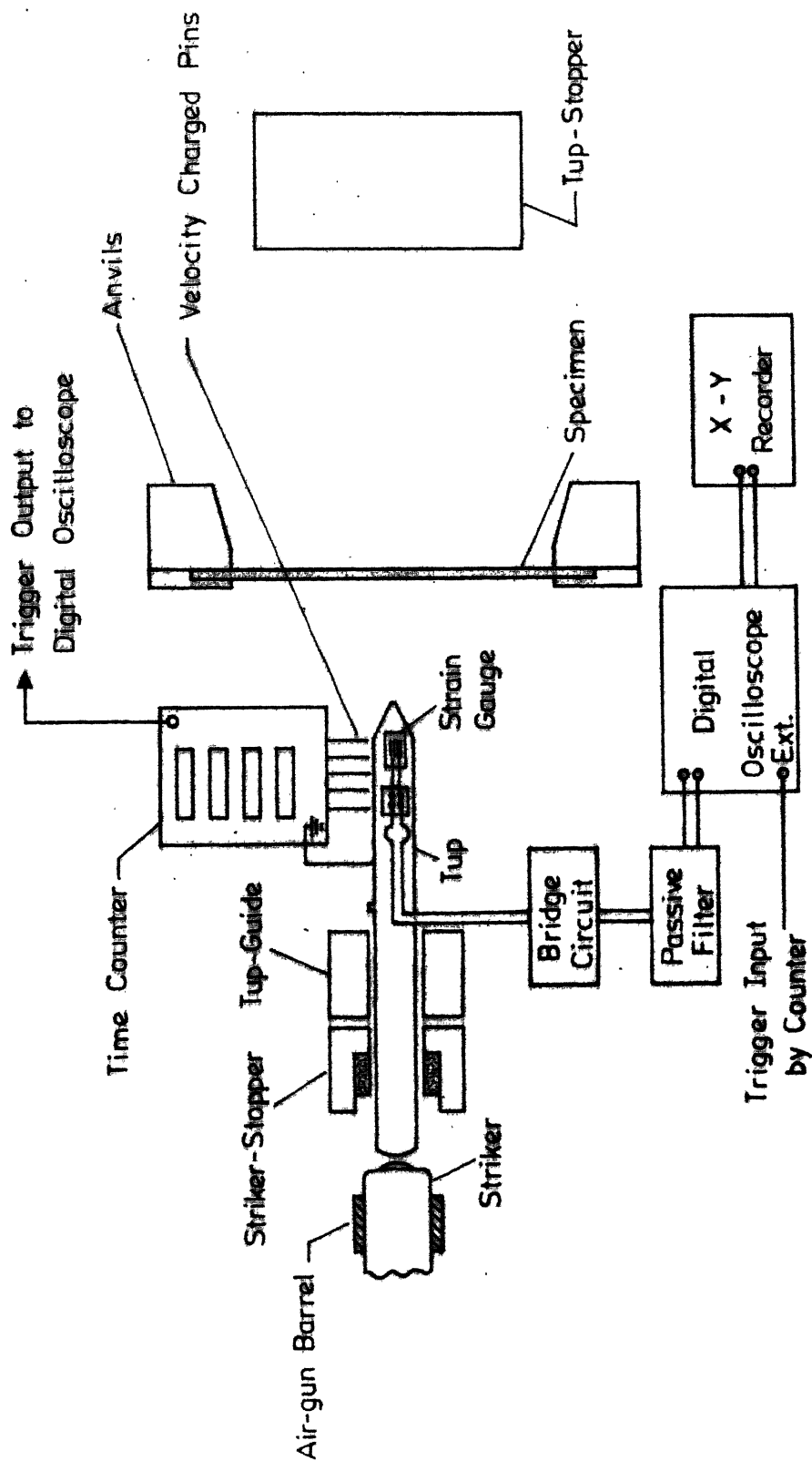


Fig. 2.4. Schematic Diagram of Tap-Impact Experimental Set-up.

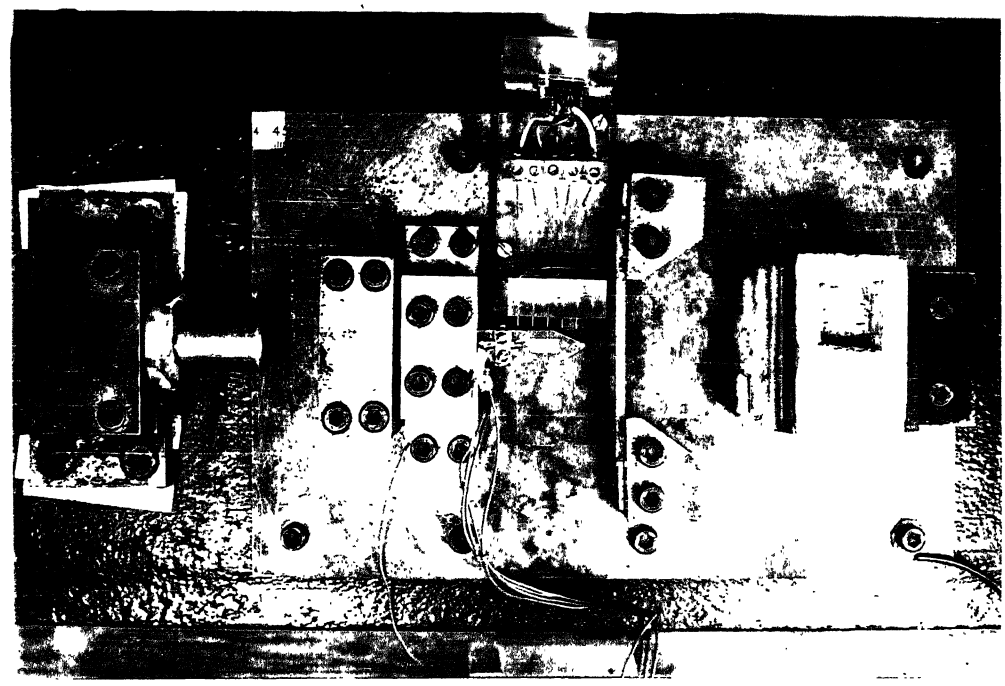


Fig. 2.5: Close View of Top-Impact Experimental Set-up

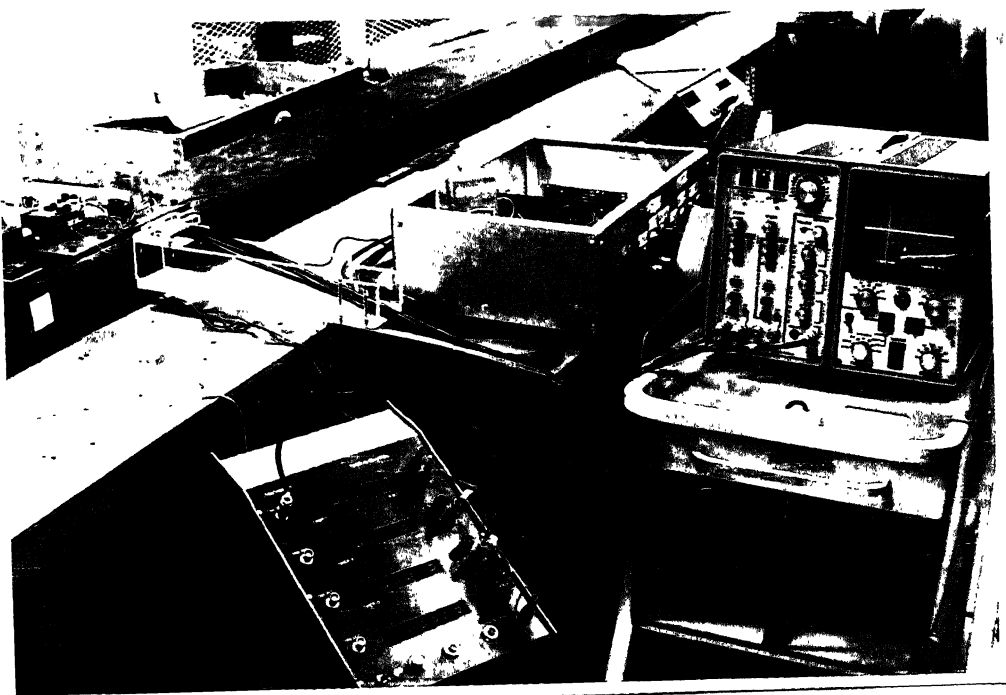


Fig. 2.6 : Overall View of Tup-Impact Experimental Set-up



specimen through a line contact. A projection of 2 mm x 2 mm is provided on one side of the tup which makes contact with velocity-pins to trigger a time counter for measuring velocity of the tup. The details of the velocity measurement device and the air-gun were described elsewhere [16]. EN-24 steel was chosen as the material of the tup. The other end of the tup where striker hits is made spherical to have point contact. The striker is stopped by a stopper. The stopper is M.S. block, having a bore with a square hole of 11 mm x 11 mm. Inside the bore rubber pad used as a damper between the striker and stopper, Fig. 2.4.

The tup motion is guided by a tup-guide having a square hole of 11 mm x 11 mm. In order to have smooth motion of the tup, the tup-guide is made of teflon and is further lubricated by machine oil. Initial location of the tup is chosen to make sure that the tup starts moving faster than the striker and separates before the striker contacts the damper and projection of the tup makes contact with velocity-pins. The location of the velocity-pins is such that it gives velocity just before the tup hits the specimen. The specimen of 120 mm long and 10 mm wide is being supported by a rigid anvils such that the unsupported length is 95.3 mm. The anvils are made of M.S. having a projection to support the specimen such that the tup makes full line contact with specimen at mid-span. A wooden tup-stopper, kept at about 90 mm away from the specimen prevents the flying off the tup

at the end of the impact. The initial velocity can be varied by varying the pressure of nitrogen gas being released to air-gun barrel. For different thicknesses, different anvils were made to have same initial distance (fixed by a spacer) of the tup from the specimen so that same impact conditions can be achieved. The firing pressure used in this experiment was 0.48 MPa. Figure 2.5 shows a close view of the tup, tup-guide, anvils and specimen.

Strain induced in the tup due to impact load is sensed by two  $120 \pm 2$  strain gauges mounted on its two opposite faces to eliminate bending effect if any. Strain gauges used are of SR-4 (Type FAE-12-12-S6EWL, gauge factor,  $S_g$  2.01). The strain gauges are mounted using epoxy and cured at  $150^\circ \text{C}$  for 4 hours in an oven. These two gauges are connected to wheatstone bridge circuit to form two active arms of the bridge through shielded wire. The shielded wire reduces the disturbance due to noise and magnetic waves. The shielding of the shielded wire and all other parts of the experimental set-up are connected to a common ground. The noise level of the system is observed 0.15 mV on an oscilloscope. The bridge circuit (Fig. 2.7), enclosed in close and grounded aluminium box, having one dummy gauge (same type as active gauge on tup) mounted on steel piece and two potentiometers so that null point can be obtained. The excitation voltage was 9 V D.C. All connections to the bridge box and oscilloscope are made with BNC connectors. For measurement of the

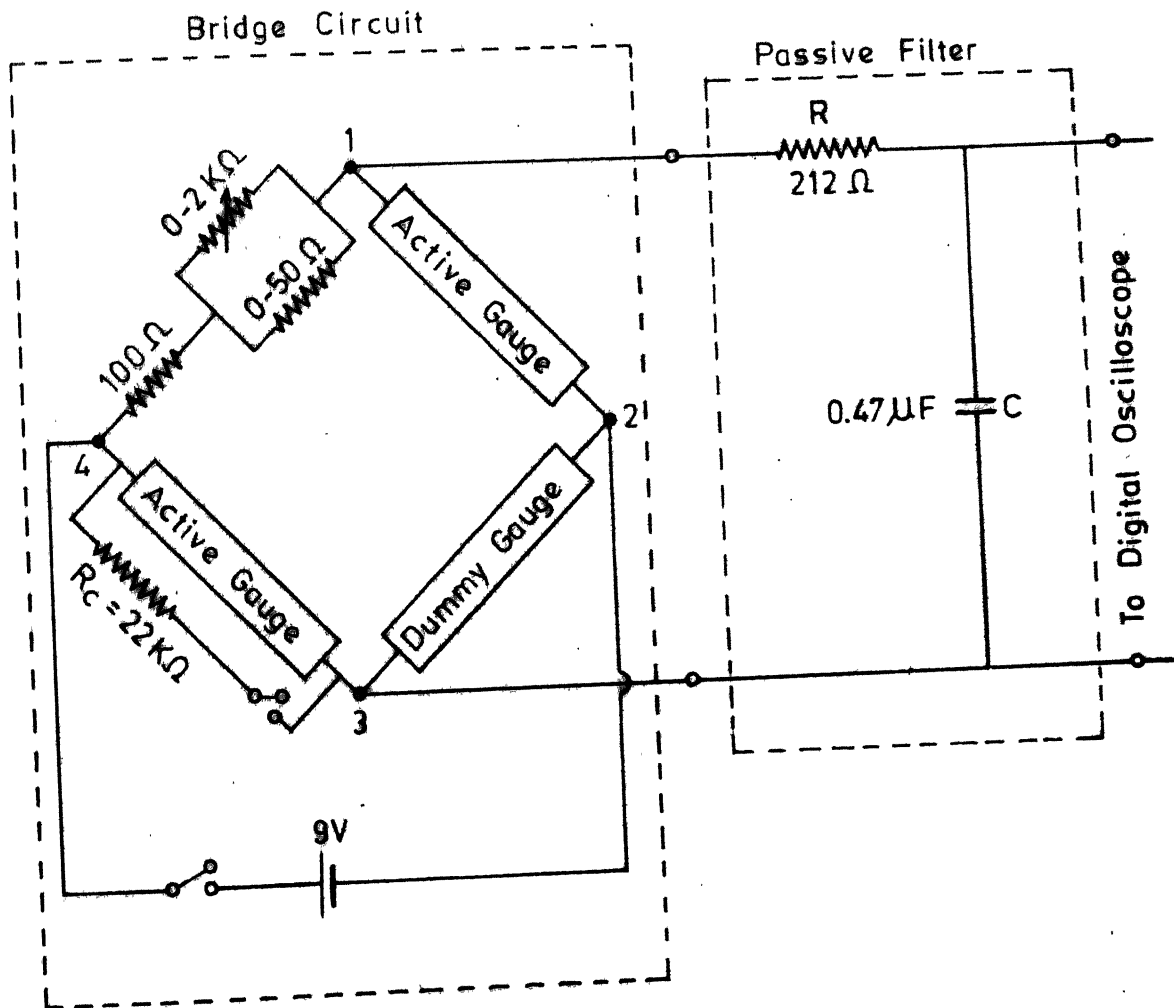


Fig. 2.7. Diagram of the Bridge Circuit with Passive Filter.

load acting in the tup, the bridge circuit is to be calibrated prior to testing. For this purpose, a calibration resistor,  $R_c$  is placed parallel to one of the active gauges. Then the voltage deflection on the oscilloscope screen corresponds to a strain given by

$$\epsilon = - \frac{R_g}{S_g (R_g + R_c)} \quad (2.1)$$

where  $S_g$  is the gauge factor of the strain gauge having resistance  $R_g$ . Since the impact load is monitored through two gauges, the output is doubled for the same strain. Using the strain, the load,  $P$  on the specimen is calculated as

$$P = AE\epsilon \quad (2.2)$$

where  $A$  is cross-sectional area and  $E$  is the Young's modulus of the tup material. The measured output voltage is equivalent to 2.9 kN/mV.

The tup is loaded at one end dynamically due to impact on the specimen and other end is free. The impact will generate compressive stress wave, at loaded end, travelling towards the free end where it is modified as the free surface can not take any stress. If the strain gauges are mounted close to the free end of the tup, for most of the time it will show very low stress. The strain gauges are mounted close to the loaded end of the tup. Hence, the strain gauges indicate mostly the impact load level existing at the specimen and tup interface, but the free end effect is

always present. As a result the signal recorded by the oscilloscope is not smooth and oscillates with a frequency of 19.23 kHz which is corresponding to the frequency of the stress wave in traversing twice the length of the tup. This undesirable effect is minimized using a passive filter (unit gain and low pass R-C type) of 10 kHz. cut-off frequency as the frequencies in the impact signal are observed to be less than 5 kHz. The passive filter can be designed for a given cut-off frequency,  $f_c$  as

$$f_c = \frac{1}{R C} \quad (2.3)$$

where  $R$  is resistance in  $\Omega$ ,  $C$  is capacitance in Farads and  $f_c$  is cut-off frequency, Hz. The capacitance of 0.47  $\mu$ F is selected and corresponding resistance of 212  $\Omega$  used for the designed cut-off frequency. The passive filter circuit is shown in Fig. 2.7.

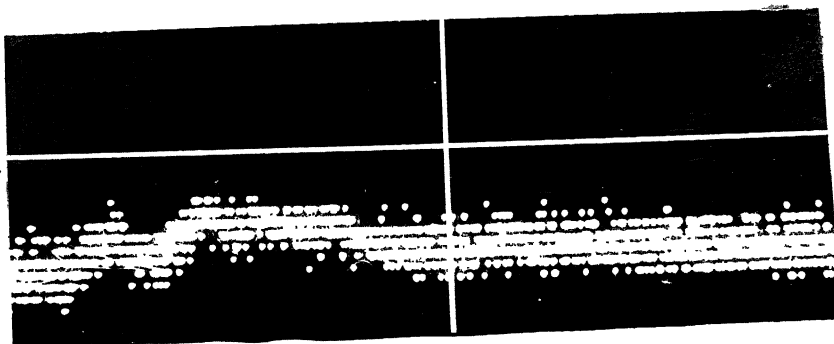
The output from the bridge circuit is connected to an oscilloscope through the passive filter. The oscilloscope is of digital type, Explorer II of Nicolet Instrument Corporation. The oscilloscope can record and store in memory an input voltage signal in the form of points (4096 points) at every 0.5  $\mu$ sec. with a least count of 0.05 mV and it has capability to expand horizontally and/or vertically a small portion (selected by a vertical cursor and horizontal cursor lines) of the stored signal and hence minute details can be studied well. The triggering position on the oscilloscope

screen can be fixed by the vertical cursor line and thus pretriggering information can be stored. The oscilloscope is triggered by a trigger-out from the time counter. The oscilloscope is triggered just before the impact starts so that the complete impact phenomena is recorded as a load history. The position of the vertical cursor line indicates the signal voltage at that instant and the same are displayed at the bottom of the oscilloscope screen. The stored signal can be recorded at variable <sup>rate</sup>/on an X - Y Recorder, using the pen-output from the oscilloscope. The recorded signal corresponds to the stored signal portion displayed on the screen of the oscilloscope.

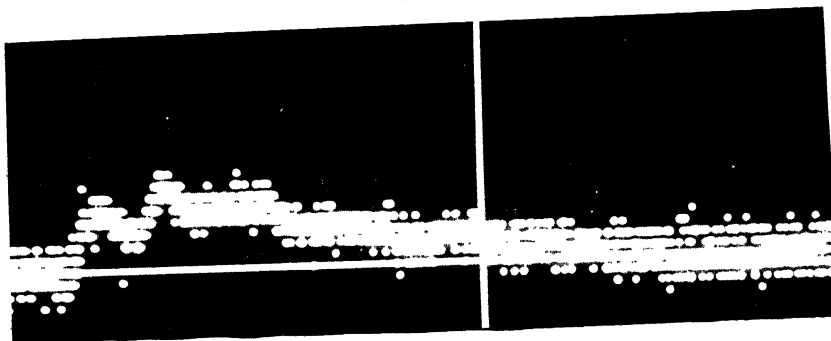
## CHAPTER 3

### RESULTS AND DISCUSSIONS

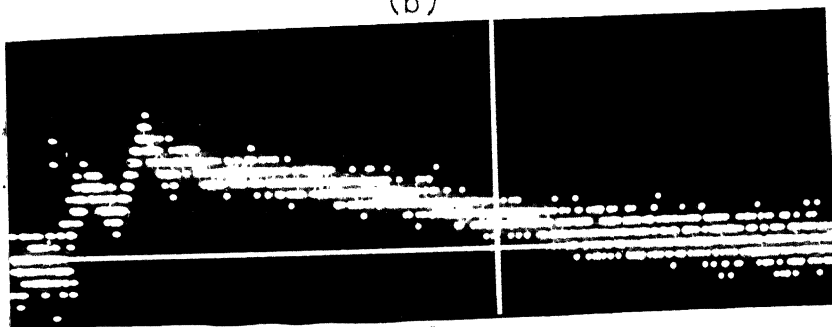
High velocity Charpy impact tests were conducted on unidirectional glass fibre-reinforced epoxy specimens with varying thickness. The impact velocity was between 24.2 and 27.4 m/sec with an average of 25.7 m/sec which is about 2 to 4 times larger than impact velocities obtained in normal drop-weight impact tests [10, 11]. The tup was instrumented so that complete load history could be recorded. The specimen thicknesses were 3.3, 4.8, 6.4 and 8.7 mm. Photographs of typical load history traces obtained on the oscilloscope are shown in Fig. 3.1 for different thicknesses. Traces appear to be wide because the oscilloscope is very sensitive and picking up noise. For the purpose of analysis, centre line of the trace was used. The load history trace was plotted on a graph paper through an X - Y Recorder hooked to the oscilloscope. Typical load history (shown schematically in Fig. 3.2) shows that initially load increases with time i.e. after the contact between the tup and the specimen load increases as the tup moves. A small kink (labelled A) is observed in the load history for all specimens. Owen [17] also observed similar kink in the load history and suggested that it is a measure of matrix cracking. Complications due to fibre pull out and fracture do not arise in such high velocity impacts. The kink is observed at about  $2/3$  of the maximum



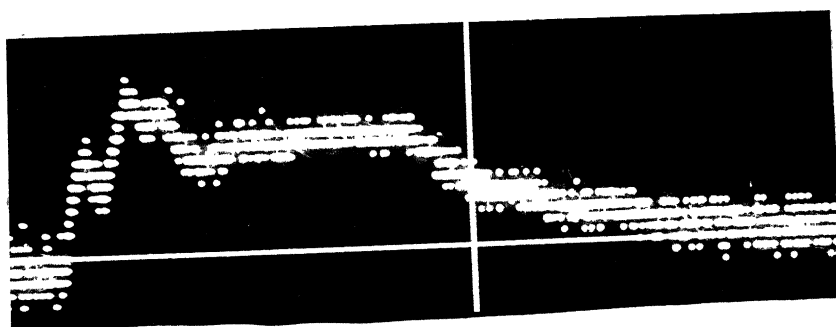
(a)



(b)



(c)



(d)

Fig. 3.1: Oscilloscope Records of Load History of Unidirectional Glass/Epoxy Composite for different Thicknesses,  $h$  (a) 3.3 mm (b) 4.8 mm (c) 6.4 mm (d) 8.7 mm.



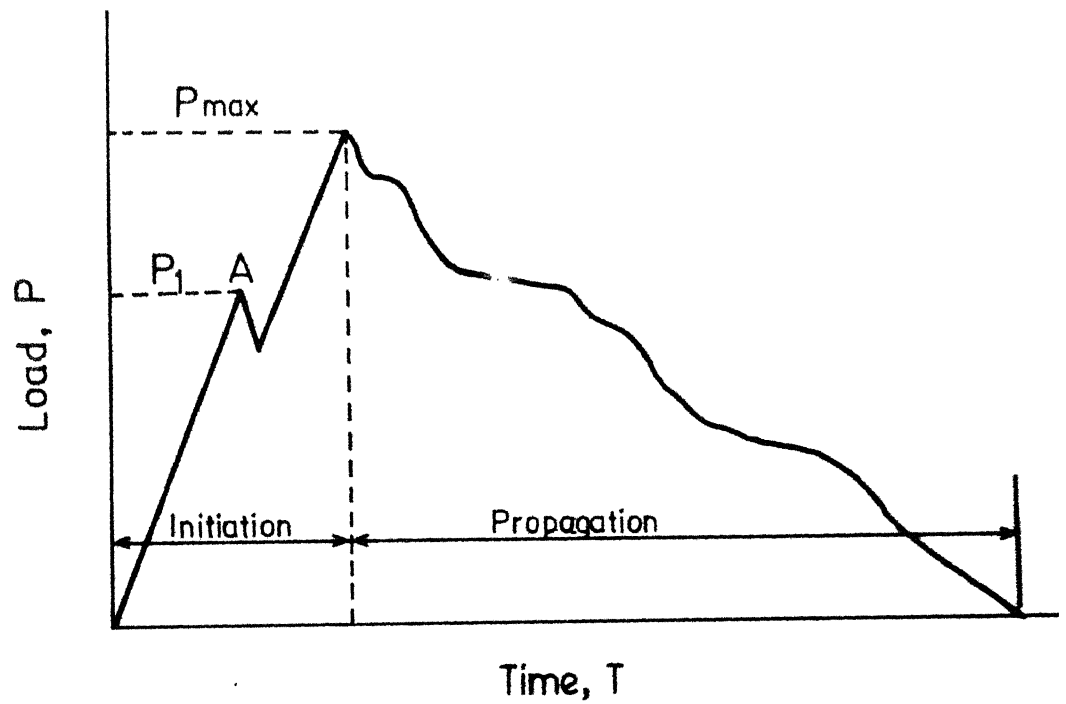


Fig. 3.2. Typical Load History During Tup Impact Test.

load. Beyond maximum load, load decreases gradually i.e., failure initiated at the peak load propagate at reduced load.

The data obtained from the load history of the specimens are given in Table 3.1 and plotted in Figs. 3.3 - 3.5. The maximum load (at which failure initiates by breaking of the fibres in the outermost layer) increases with specimen thickness (Fig. 3.3). However, the increase in maximum load is linear with the specimen thickness and not proportional to the <sup>square of the</sup> thickness as is expected from static strength considerations. This apparent discrepancy will be explained later through the consideration of failure mode. Maximum tensile stress and shear stress are plotted in Fig. 3.4. The high shear stress developed in the thick specimens results in the shear failure preceding the tensile failure as will be explained later alongwith the damage propagation study.

Initiation time, propagation time and total impact duration are shown in Fig. 3.5. The initiation time (corresponding to the maximum load) decreases as the thickness increases because thick specimens require smaller displacements to develop the same stresses (ultimate strength of fibres) in the outermost layers whereas the tup velocity at the time of contact with the specimen is same in all cases. In addition, the strength of the specimen decreases with

TABLE 3.1  
RESULTS OF LOAD-HISTORY OF IUP IMPACT TEST

Specimen No.	Specimen Thickness mm	Load at First Kink $P_1$ kN	Peak Load $P_{max}$ kN	* $\sigma_{max}$ MPa	** $\tau_{max}$ MPa	Initiation Time $t_i$ $\mu$ sec	Propagation Time $t_p$ $\mu$ sec	Total Impact Duration $t_t$ $\mu$ sec
1	3.26	0.322	0.465	626	21.4	516	1155	1671
2	3.27	0.465	0.501	670	23.0	546	1257	1803
3	3.24	0.405	0.642	850	29.7	512	1248	1760
4	3.29	0.516	0.775	1023	35.3	536	1250	1786
5	3.26	0.408	0.579	778	26.6	502	1367	1869
6	4.81	0.681	1.021	631	31.8	405	1587	1992
7	4.82	0.714	1.055	649	32.8	397	1796	2193
8	4.81	0.681	1.123	694	35.0	397	1859	2256
9	4.81	0.721	1.064	657	33.2	415	1725	2140
10	4.82	0.755	1.098	676	34.2	407	1849	2256
11	6.45	1.004	1.630	560	37.9	330	1920	2250
12	6.39	1.004	1.592	557	37.4	336	2228	2564
13	6.43	1.073	1.523	527	35.5	337	2128	2465
14	6.45	1.038	1.453	499	33.8	340	2208	2548
15	6.36	1.038	1.453	514	34.3	337	2227	2564
16	8.71	1.593	2.182	411	35.6	281	3276	3557
17	8.77	1.142	2.007	373	34.3	281	3383	3664
18	8.71	1.315	2.076	391	35.8	277	3363	3640
19	8.73	1.419	2.422	454	41.6	582	3008	3590
20	8.74	1.419	2.111	395	36.2	287	3139	3426

$$* \sigma_{max} = \frac{3}{2} \frac{P_{max} L}{bh^2}$$

$$** \tau_{max} = \frac{3}{2} \frac{P_{max}}{bh}$$

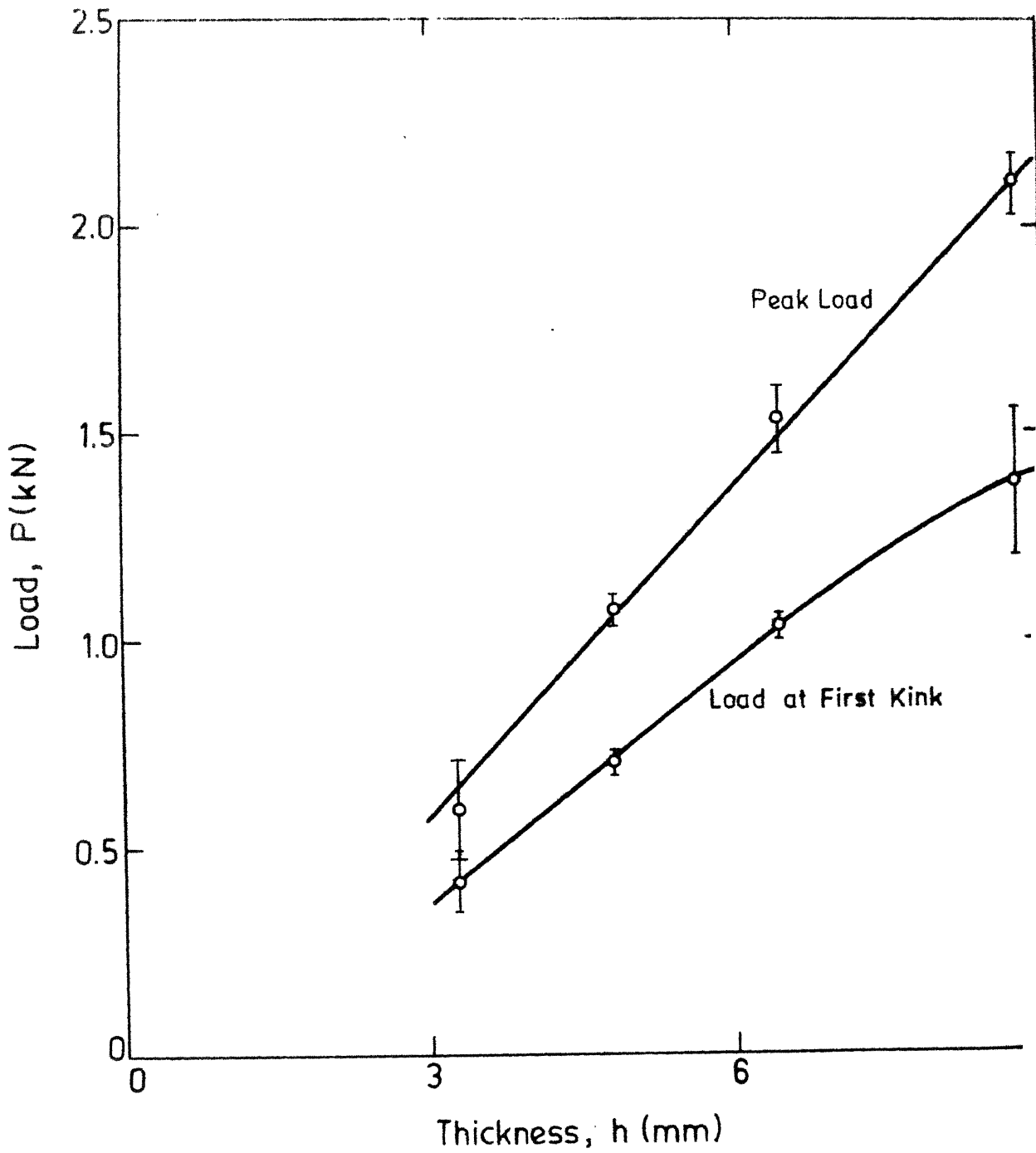


Fig. 3.3. Impact Load Vs Thickness.

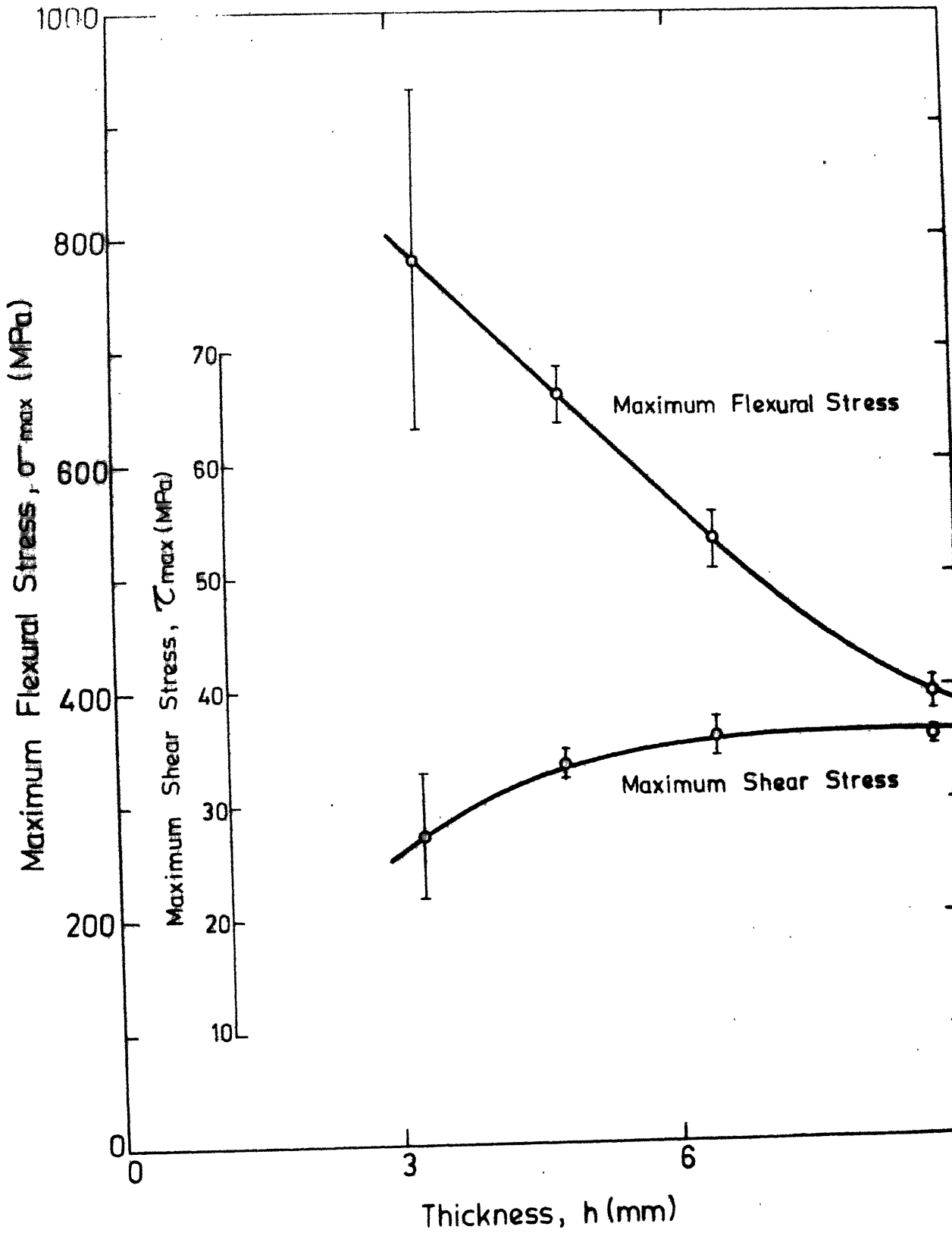


Fig. 3.4. Stress at Peak Load Vs Thickness.

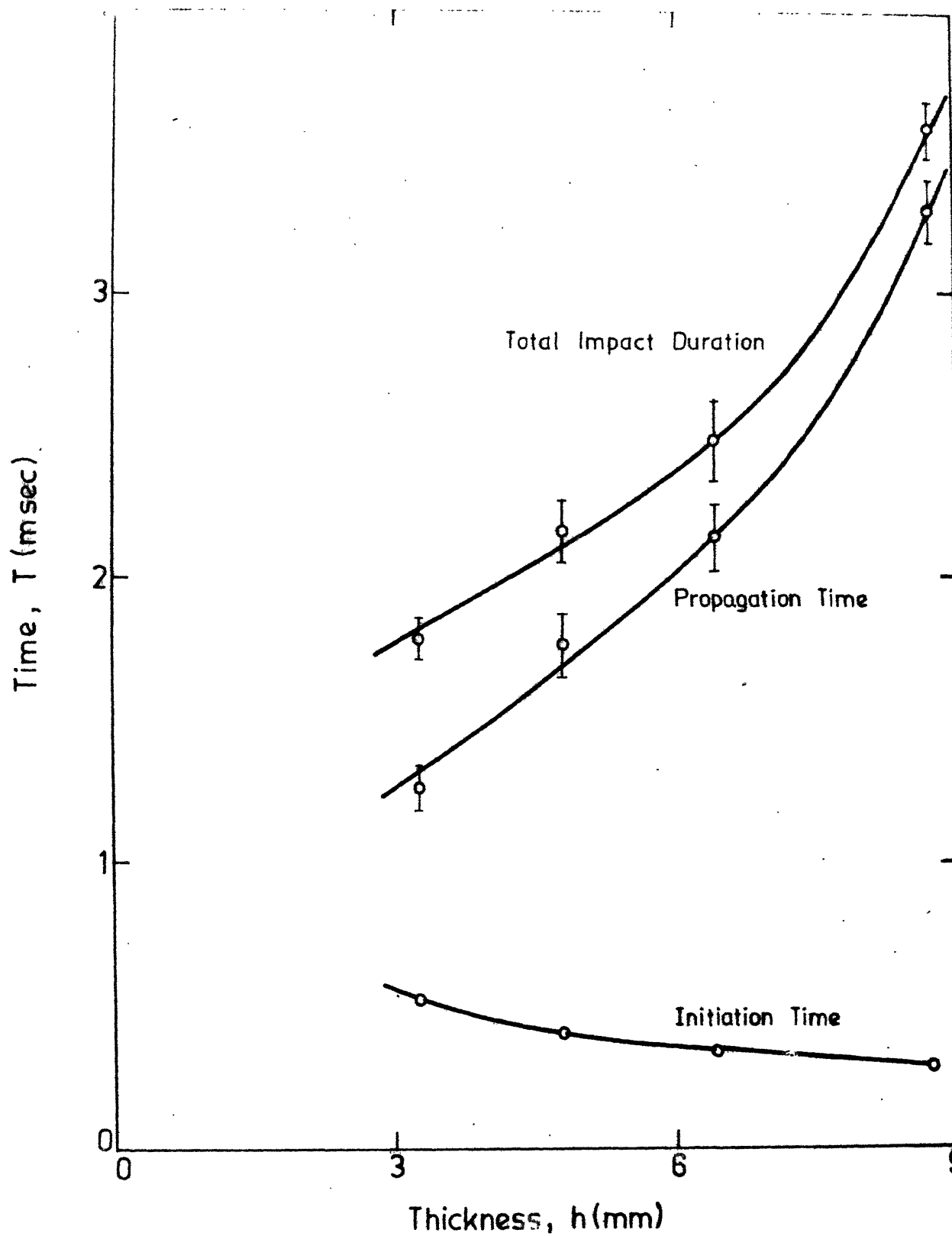


Fig. 3.5. Time Vs Thickness.

increase in thickness as explained earlier. Propagation time and total duration of impact, as expected, increases with thickness.

The knowledge of load history and initial tup velocity can be used to calculate energy absorbed by the specimen at any instant. It can be shown that the energy absorbed by the specimen is [18]:

$$E = E_a \left(1 - \frac{E_a}{4 E_0}\right) \quad (3.1)$$

where

$$E_a = v_0 \int P \, dt ,$$

$$E_0 = \frac{1}{2} m v_0^2$$

In the Eqn. 3.1,  $m$  is the mass of the tup,  $v_0$  its initial velocity so that  $E_0$  is the initial kinetic energy of the tup.

$\int P \, dt$  is the area under the load history curve and, therefore,  $E_a$  is usually referred to as the apparent energy. Using the Eqn. 3.1, the energy is calculated for the point corresponding to the peak load and the point at which the fracture is completed. The energies thus obtained are referred to as the initiation and total impact energies respectively. Difference between the two energies is called the propagation energy.

Initiation energy,  $E_i$ , propagation energy,  $E_p$ , and the total energy,  $E_t$ , are given in Table 3.2 and plotted in Fig. 3.6. All the three energies,  $E_i$ ,  $E_p$  and  $E_t$ , increase

TABLE 3.2  
IMPACT PROPERTIES OF UNIDIRECTIONAL GFRP

Specimen No.	Specimen Thickness mm	Initiation Energy $E_i$ J	Propagation Energy $E_p$ J	Total Energy $E_t$ J	Ductility Index DI
1	3.26	3.23	6.77	10.00	2.09
2	3.27	4.69	8.37	13.06	1.79
3	3.24	3.81	10.94	14.76	2.87
4	3.29	4.78	12.88	17.66	2.70
5	3.26	3.09	8.32	11.41	2.70
6	4.81	5.46	12.33	17.79	2.26
7	4.82	6.20	18.15	24.35	2.93
8	4.81	5.98	18.02	24.00	3.02
9	4.81	6.26	17.10	23.36	2.73
10	4.82	6.27	16.84	23.11	2.69
11	6.45	7.27	19.44	26.70	2.68
12	6.39	7.00	25.33	32.33	3.62
13	6.43	7.74	21.16	28.84	2.73
14	6.45	7.35	19.78	27.13	2.69
15	6.36	7.08	22.50	29.58	2.96
16	8.71	9.74	30.58	40.32	3.14
17	8.77	8.15	32.21	40.36	3.95
18	8.71	8.18	32.15	40.33	3.93
19	8.73	23.14	17.22	40.36	0.74
20	8.74	8.96	31.23	40.19	3.49



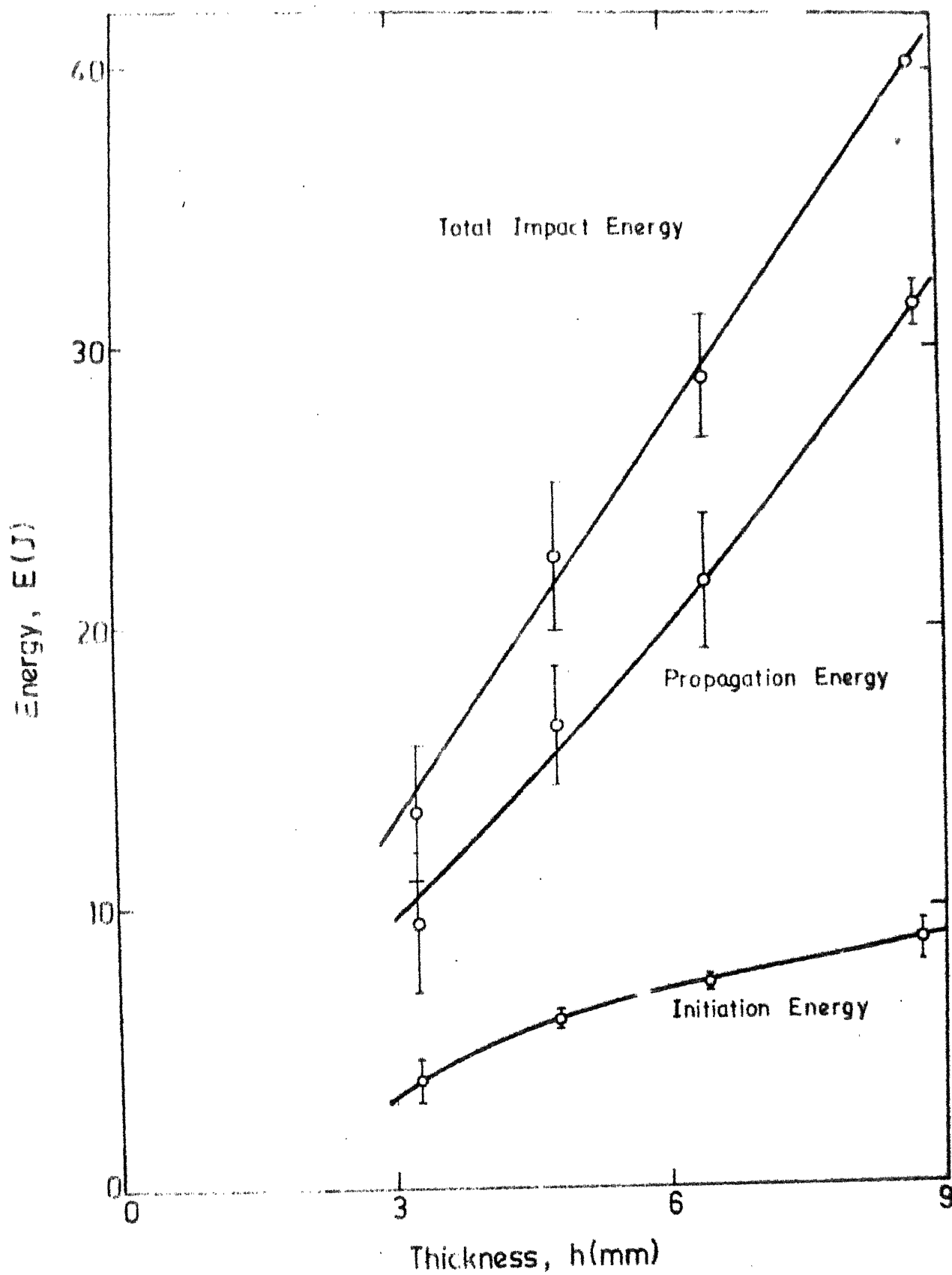


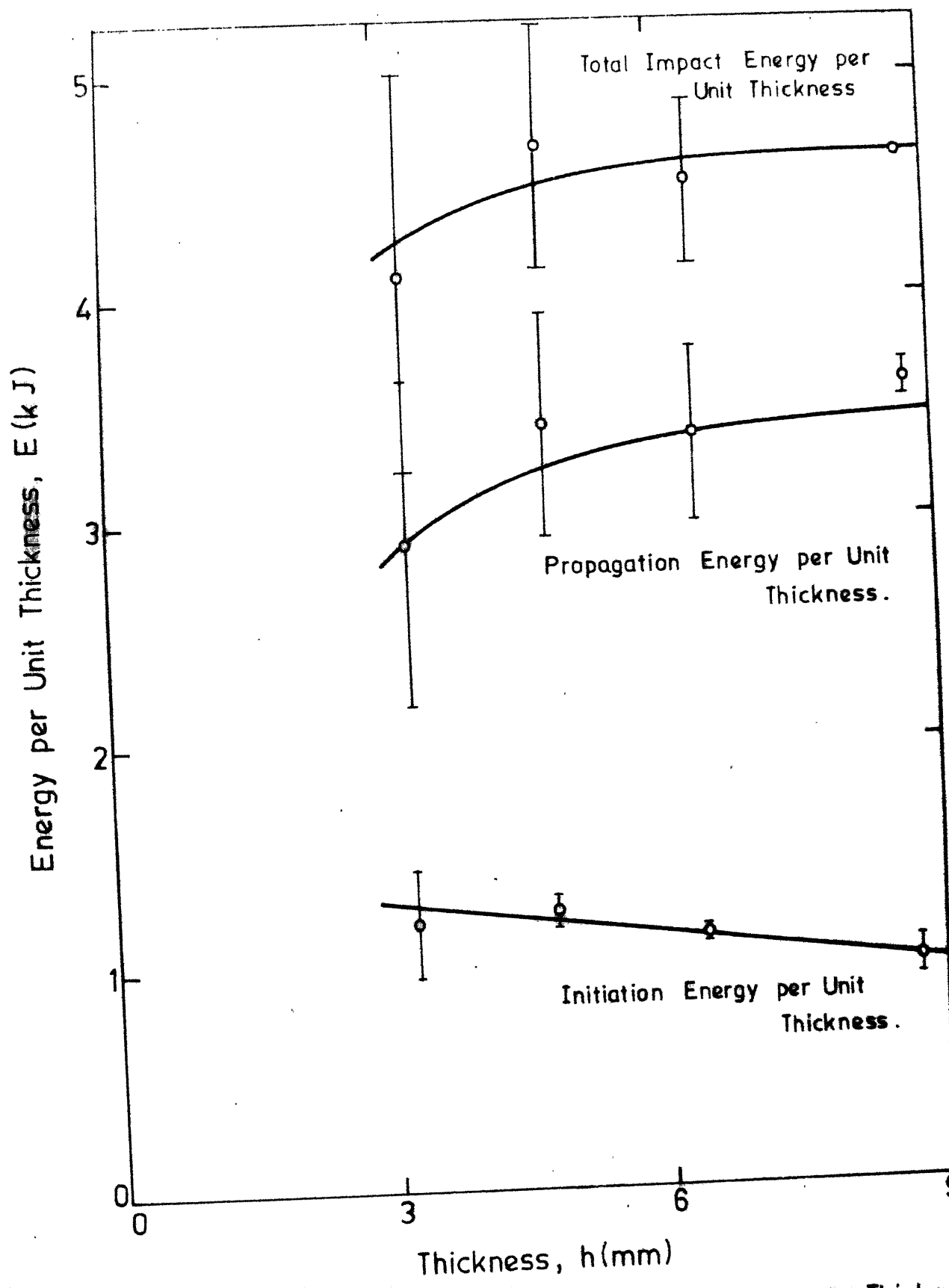
Fig 36. Effect of Thickness on Energy Absorbed by GFRP

with thickness. However, propagation energy appears to increase much more compared to the initiation energy. It is also observed that the scatter in propagation energy is also larger than that in initiation energy. This may be expected because the propagation energy depends upon the damage mode. It will be shown later that there is a large variation in the damage mode from one specimen to another.

The initiation, propagation and total energies per unit thickness are shown in Fig. 3.7. The initiation energy per unit thickness decreases as the thickness increases while propagation and total energies per unit thickness increases. However, the increase is much smaller than that in non-normalized energies. For ranking the composite materials a term called the "ductility index" is commonly used. Introduced by Beaumont et al. [6], the ductility index, DI, is defined as the ratio of propagation energy to initiation energy:

$$DI = \frac{E_p}{E_i} \quad (3.2)$$

The ductility index is also given in Table 3.2 and plotted against thickness in Fig. 3.8. The ductility index increases slightly with thickness. The increase may be due to change in span-to-thickness ratio (i.e. due to geometric change in test configuration) rather than a change in the material behaviour. The values of ductility index (ranging from 2.43 to 3.05) obtained here are much higher than 0.37 as



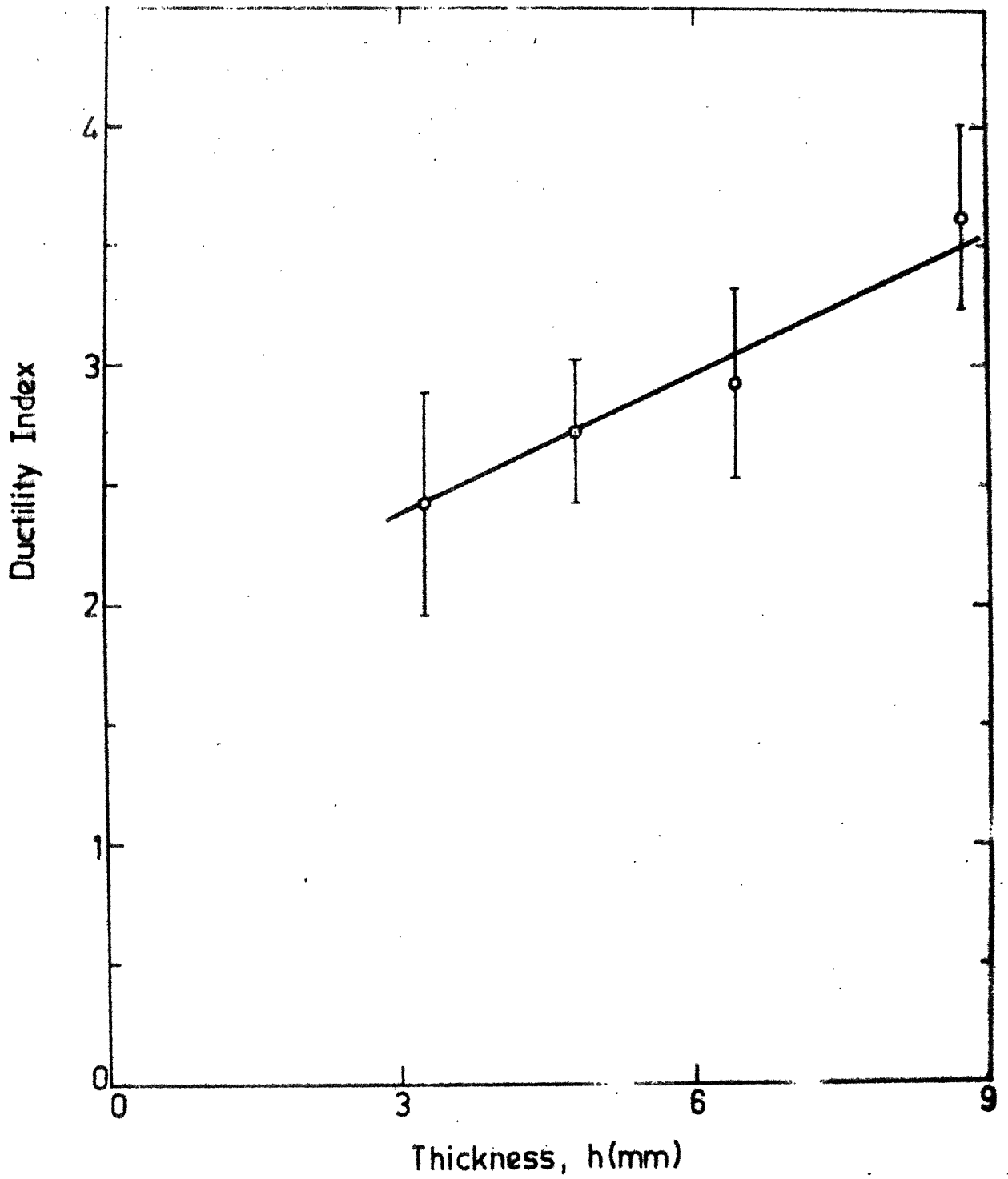
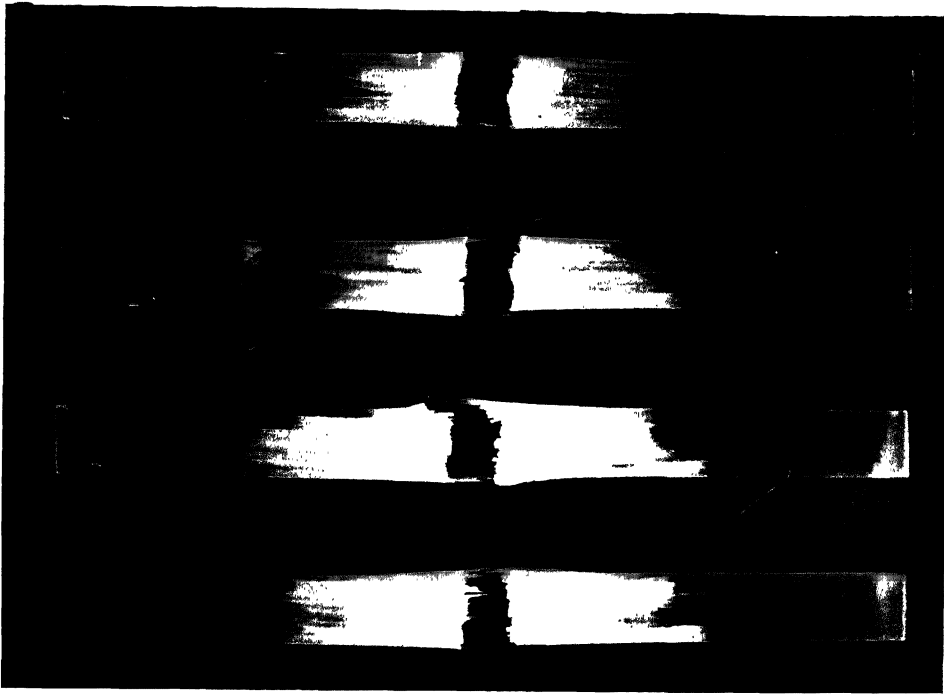


Fig. 3.8. Variation of Ductility Index with Thickness.

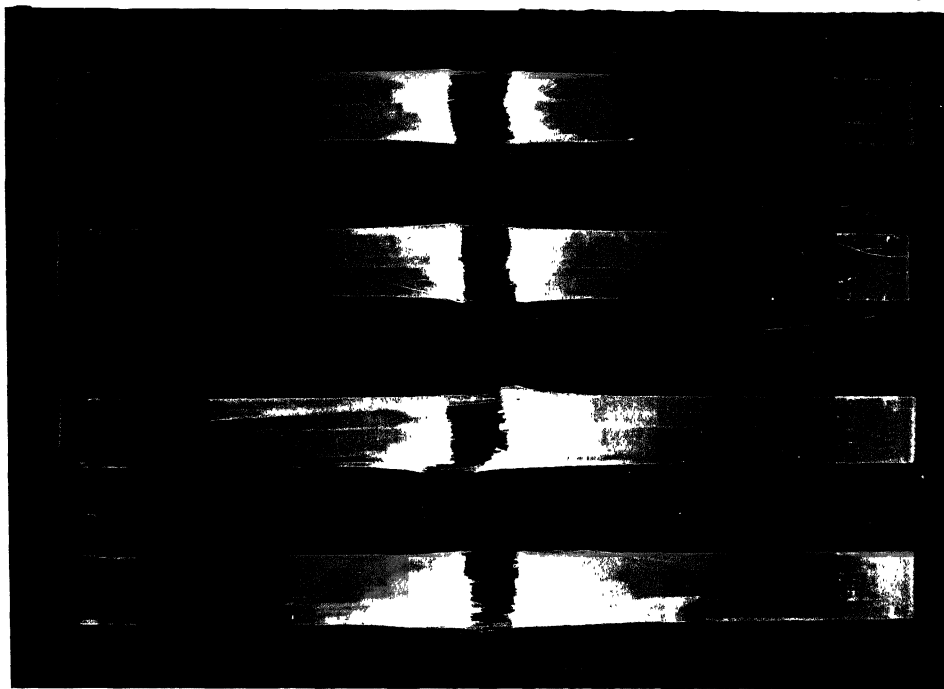
reported by Mallick and Broutman [12] for a similar unidirectional glass fibre composites. There appears to be inconsistency in their results which show a lower ductility index for glass fibre composite than for carbon fibre composite. The ductility index obtained here is more tangible in that it is higher than that for carbon and Kevlar Fibre composites as reported by Mallick and Broutman.

After the tests, the impact specimens were examined to study the damage and failure mechanisms and also for a possible correlation between the observed dynamic strength and damage mode. Specimens with thickness 3.3 mm generally fractured in two pieces through fibre breaking (Fig. 3.9). There is also extensive delamination failure adjacent to the fracture plane as is indicated by whitened portion of the specimen in the photograph. It is further observed that the delamination failure is more extensive on the compression side than on the tension side. Contact pressure on the compression side causes local damage before fibre failure on the tension side and thus is probably responsible for greater delamination failure on the compression side.

Specimens with thickness 4.8 mm also generally fail in two pieces (Fig. 3.10) and show a general damage behaviour similar to the 3.3 mm thick specimen. However, one specimen shows shear failure preceding the fibre failure. The shear failure becomes more predominant in thicker



(a)



(b)

Fig. 3.9: Photographs of the Two Sides of 3.3 mm Thick  
Unidirectional Impact Specimens  
(a) Compression Side (b) Tension Side

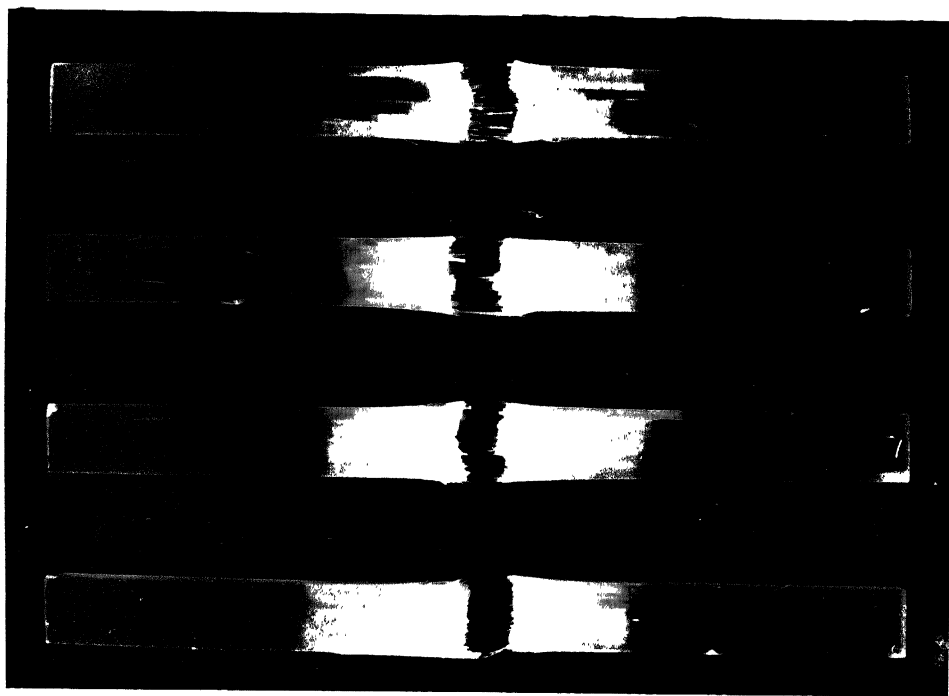


Fig. 3.10: Photograph of Compression Side of 4.8 mm  
Thick Unidirectional Impact Specimens

specimens where the shear failure is observed in all specimens. Damage behaviour of 6.4 and 8.7 mm thick specimen is shown in Figs. 3.11 and 3.12. The difference in the damage behaviour is primarily due to the shear failure which is caused by the reduced span-to-thickness ratio. For 3.3 mm thick specimen, this ratio is about 29 while for 8.7 mm thick specimen it is less than 11. The decrease in span-to-thickness ratio causes an increase in the maximum shear stress to maximum tensile stress ratio and consequently increases the tendency for shear failure preceding the tensile failure.

Shear failure observed in the thick specimens reduces the maximum load that the specimen can sustain. After shear failure the specimen can not be considered as one thick specimen but it should be considered as two specimens acting together to carry the load. The maximum load, therefore, corresponds to the tensile failure of one or both of these parts of the specimen. The dynamic tensile strength of the material can be obtained more accurately if the shear failure is accounted for. The corrected dynamic strength is shown in Fig. 3.13. In calculating the strength it has been assumed that the shear failure preceding the tensile failure causes the specimen to split in two pieces at the neutral plane. A small variation in the dynamic strength is due to the fact that the shear failure is not always at the neutral plane and it is not always a single well defined plane.



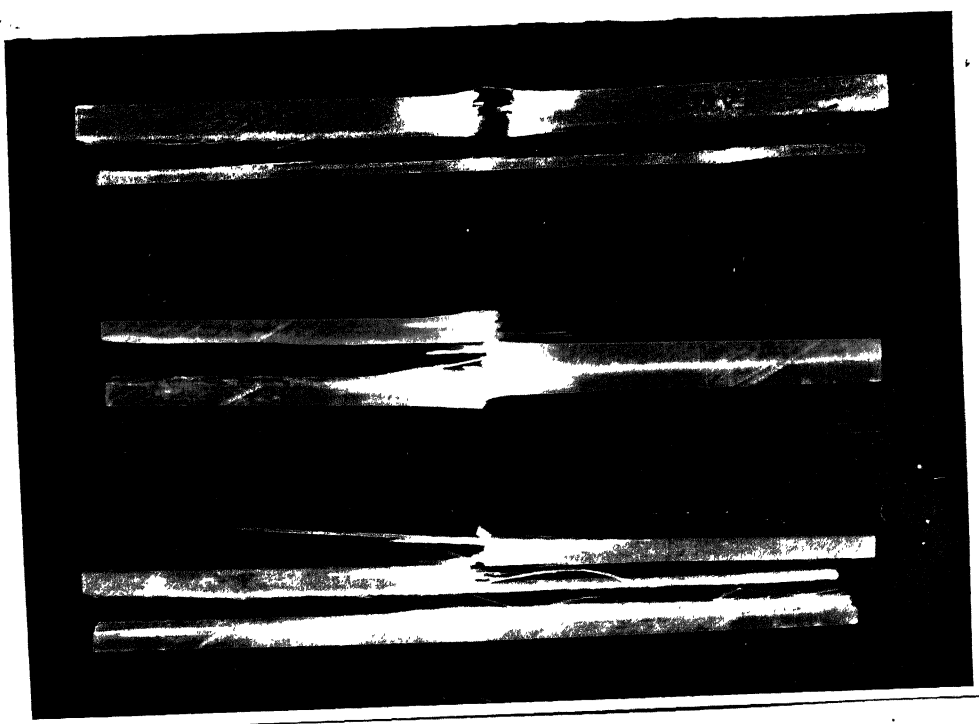


Fig. 3.11: Side View of 6.4 mm Thick Unidirectional Impact Specimens



Fig. 3.12: Side View of 8.7 mm Thick Unidirectional Impact Specimens

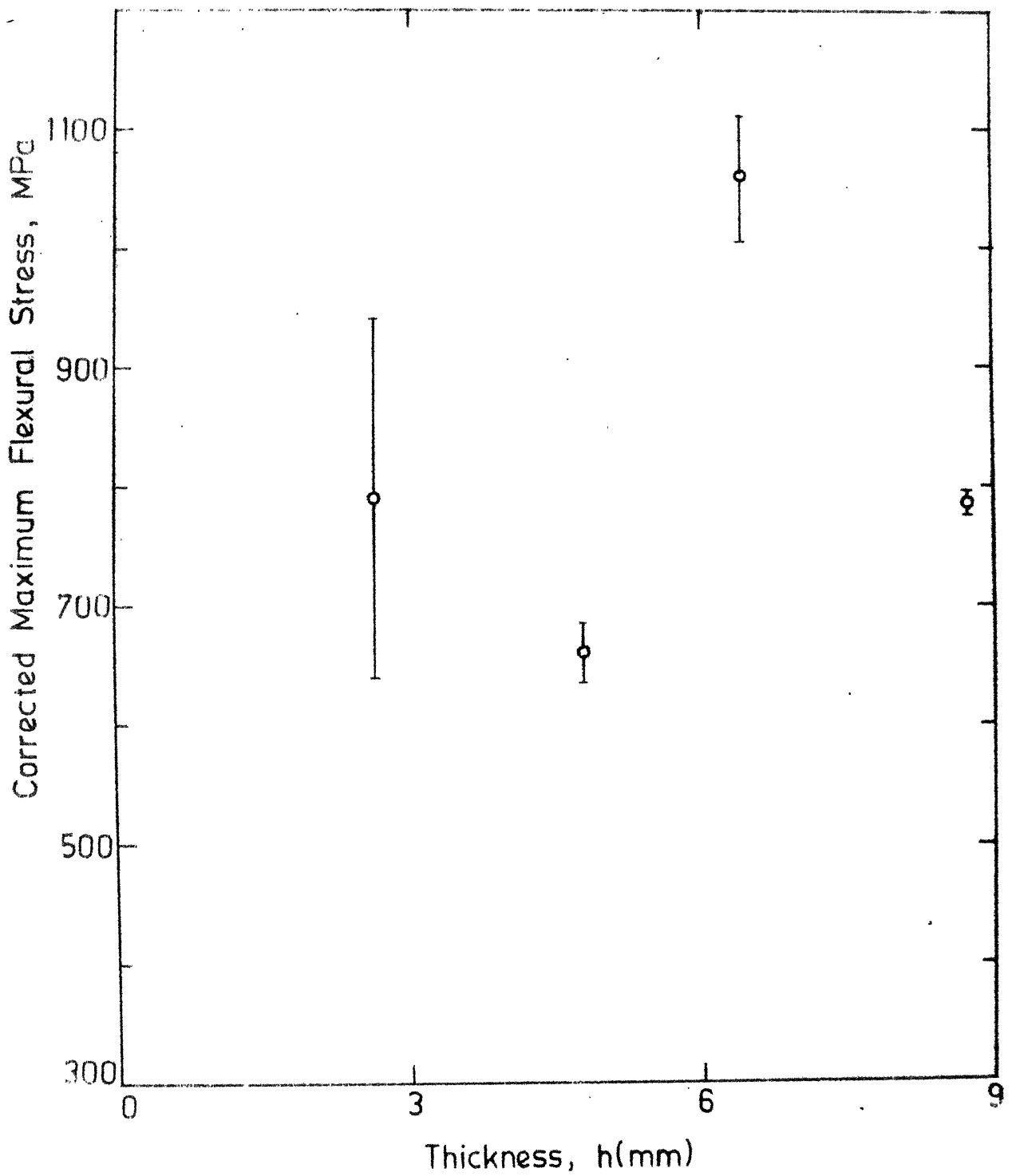


Fig. 3.13. Corrected Maximum Flexural Stress Vs Thickness.

## CHAPTER 4

### SUMMARY AND CONCLUSIONS

High velocity impact properties of unidirectional GFRP have been investigated. The specimens were obtained from a unidirectional GFRP plate (fibre volume fraction, 43.3%) fabricated using filament winding machine which was designed and fabricated for this purpose. The filament winding machine is capable of casting unidirectional composite plates of different thicknesses (upto 21 mm) and different fibre volume fraction. To perform the impact tests an instrumented impact testing machine was designed and fabricated in which a tup (projectile) was accelerated by a striker through an air-gun to obtain high impact velocities. The impact velocity can be varied using different gas pressures in the air-gun. The load on specimen was monitored by strain gauges mounted on the tup and was recorded on a digital oscilloscope, Explorer II of Nicolet Instrument Corporation, through a passive filter. For the purpose of analysis, the load history was recorded on graph paper using an X-Y Recorder (Hewlett-Packard) hooked to the digital oscilloscope. The specimen were unnotched Charpy type of four different thicknesses.

The study of the impact data indicates maximum load increases linearly with thickness rather than proportional to the square of the thickness. The testing machine gives a measure of matrix cracking as indicated by a kink

in the load history. The time to reach the maximum load decreases with thickness.

The propagation energy increases much more compared to initiation energy and the ductility index increases slightly with thickness. The increase in ductility index may be due to change in span-to-thickness ratio. Thinner specimen show extensive delamination failure on the compression side and fail across the fibres while thick specimen show extensive shear failure along with fibre breakage. Shear stress at maximum load increases with thickness, but the flexural stress at maximum load decreases, thus, causes shear failure in thick specimen and hence, the specimen can not be considered as one thick specimen. For comparing the Charpy impact data of different fibre material span-to-thickness ratio becomes an important aspect and should be high enough to ensure the failure across the fibres.

The testing machine is capable of varying impact velocity over a wide range compared to normal drop-weight impact tests and it gives a measure of matrix cracking. So the investigation may be continued further for different constituent materials, fibre orientation, matrix materials, other manufacturing variables and specimen geometry as the instrumented impact data is not available in literature at such high velocity.

## REFERENCES

1. Chamis, C.C., Hanson, M.P. and Serafini, T.T., "Designing for Impact Resistance with Unidirectional Fiber Composites", NASA TN D-6463, August 1971.
2. Novak, R.C. and DeCrescente, M.A., "Impact Behavior of Unidirectional Resin Matrix Composites Tested in Fiber Direction", Composite Materials: Testing and Design, (Second Conference), ASTM STP 497, American Society for Testing and Materials, 1972, pp. 311-323.
3. Prewo, K.M., "The Charpy Impact Energy of Boron-Aluminum", J. Compos. Mater., 6, October 1972, pp. 442-455.
4. Agarwal, B.D. and Narang, J.N., "Strength and Failure Mechanism of Anisotropic Composites", Fibre Sci. Technol., 10(1), 1977, pp. 37-52.
5. Toland, R.H., "Instrumented Impact Testing of Composite Materials", ASTM STP 563, American Society for Testing and Materials, Philadelphia, Pa., 1974, pp. 133-145.
6. Beaumont, P.W.R., Riewald, P.G. and Zweben, C., "Methods for Improving the Impact Resistance of Composite Materials", in Foreign Object Impact Behavior of Composites, ASTM STP 568, American Society for Testing and Materials, 1974, pp. 134-158.

7. Beaumont, P.W.R. and Server, W.L., "Some Observations on the Dynamic Fracture Behavior of Carbon Fiber - Strengthened Epoxy Resin", Composite Reliability, ASTM STP 580, American Society for Testing and Materials, 1975, pp. 443-457.
8. Adams, D.F. and Miller, A.K., "An Analysis of the Impact Behavior of Hybrid Composite Materials", Mater. Sci. Eng., 19, 1975, pp. 245-260.
9. Pike, R.A. and Novak, R.C., "The Pendulum Test: A Method for Assessing the Impact Response of Composite Material," SPI, 31st Annual Technical Conference, Washington, D.C., February 1976, Section 12-D.
10. Broutman, L.J. and Rotem, A., "Impact Strength and Toughness of Fiber Composite Material", in Foreign Object Impact Damage to Composite, ASTM STP 568, American Society for Testing and Materials, Philadelphia, Pa., 1975, pp. 114-133.
11. Mallick, P.K. and Broutman, L.J., "Impact Properties of Laminated Angle Ply Composites", SPI, 30th Annual Technical Conference, Washington, D.C., 1975, Section 9-C.
12. Mallick, P.K. and Broutman, L.J., "Static and Impact Properties of Hybrid Composites", J. Test. Eval., 5(3), 1977, pp. 190-200.

13. Yeung, P. and Broutman, L.J., "The Effect of Glass - Resin Interface Strength on the Impact Strength of Fiber Reinforced Plastics", Polym. Eng. Sci., 18(2), 1978, pp. 62-72.
14. Aleszka, J.C., "Low Energy Impact Behavior of Composite Panels", J. Test. Eval., 6(3), 1978, pp. 202-210.
15. Labor, J.D., "Impact Damage Effects on the Strength of Advanced Composites", Nondestructive Evaluation and Flaw Criticality for Composite Materials, ASTM STP 696, R.B. Pipes, Ed., American Society for Testing and Materials, 1979, pp. 172-184.
16. Chimmalgi, V.S., "Experimental Study of Stress-Strain Behaviour of Epoxy at High Strain Rate", M.Tech. Thesis, Department of Mechanical Engineering, I.I.T. Kanpur, 1981.
17. Owen, G.E. Jr., "A Comparison of Impact Tests for Assessment of Fiberglass Reinforced Plastic Toughness", Polym. Eng. Sci., 21(8), 1981, pp. 467-473.
18. Agarwal, B.D. and Broutman, L.J., "Analysis and Performance of Fiber Composites", John Wiley and Sons, New York, 1980, pp. 250.